Supporting Information

Engineered from waste: ionic liquid processing of keratin for 3D printing biomedical scaffolds

Cariny Polesca[1,2†], Rita Sobreiro-Almeida[1,†,*], Helena Passos[3,4], João A. P. Coutinho[1], Jason P. Hallett[2], João F. Mano[1*], Mara G. Freire[1,*]

[1] CICECO – Aveiro Institute of Materials, Department of Chemistry, University of Aveiro, Aveiro 3810-193, Portugal;

[2] Department of Chemical Engineering, Imperial College London, South Kensington Campus, London SW7 2AZ, UK;

[3] ALiCE – Associate Laboratory in Chemical Engineering, Faculty of Engineering, University of Porto, Porto 4200-465, Portugal;

[4] LSRE-LCM – Laboratory of Separation and Reaction Engineering – Laboratory of Catalysis and Materials, Faculty of Engineering, University of Porto, Porto 4200-465, Portugal.

* corresponding authors: rita.almeid@ua.pt , jmano@ua.pt and maragfreire@ua.pt

† Authors contributed equally.

Experimental Methods

Materials

White chicken feathers (WF) were collected from Campoaves Company in Oliveira de Frades, Portugal. Brown chicken feathers (BF) were collected from a local poultry farmer in Portugal. The feathers were pre-treated before dissolution, as previously reported [1]. Briefly, chicken feathers were washed 3 times with soap and dried at 50 °C. The feathers were milled and immersed in ethanol 99% for 24 h to remove the fatty matter. Then, the cleaned wet feathers were dried at 50 °C and then stored in plastic bags at 5 °C until further use. $[N_{111(2OH)}][C_1CO_2]$ (>98 wt%) and $[C_2C_1im][C_1CO_2]$ (>98 wt%) were purchased from IOLITEC. All the other materials used in this work were acquired from Sigma Aldrich unless otherwise stated.

Chicken feathers dissolution (ink preparation)

White and brown chicken feathers were dissolved in $[N_{111(2OH)}][C_1CO_2]$ or $[C_2C_1im][C_1CO_2]$ (80 wt% in water) at 100 °C, 650 rpm for 4 h in a solid: liquid (chicken feather: solvent) ratio of 1: 20 w/w in a carrousel (Carousel Tech, Radleys). Then, the solution was moved to a falcon tube and centrifuged at 2000 rpm for 5 min in a refrigerator centrifuge machine (Megafuge 16R, Thermo Fischer).

Support bath preparation

The support bath was prepared by adding 0.5 g of agarose and 11 mM of calcium chloride ($CaCl_2$) to 100 mL of carbonate-bicarbonate buffer (0.8 M). The bath was microwaved for 1 min and cooled down to room temperature under constant agitation at 700 rpm to form agarose microparticles. The solution was stored in the fridge (4 °C) until it was used for rheological characterisation or the collection and crosslinking of scaffolds.

Rheological characterisation

The viscoelastic properties of all solutions (WF + $[N_{111(2OH)}][C_1CO_2]$, BF + $[N_{111(2OH)}][C_1CO_2]$, WF + $[C_2C_1im][C_1CO_2]$ and BF + $[C_2C_1im][C_1CO_2]$) as well as the support bath were characterised on a rheometer (Kinexus Lab$^+$, Malvern Panalytical, UK), using a 20 mm diameter parallel-plate, and 1 mm gap. All tests were performed at 25 °C. Sweep strain tests were executed to study variations in the storage (elastic) modulus (G') and the viscous (loss) modulus (G'') within the linear viscoelastic region from a low shear strain of 0.1 % until 1000 %, at 1.0 Hz frequency. The shear-thinning behaviour was conducted to assess viscosity by varying the shear rates from 0.1 to 100 s^{-1}. Furthermore, step strain tests were performed to measure the self-healing ability of the support bath at a constant frequency of 1 Hz, with strain intervals varying from 1% to 100% during 5 consecutive cycles of 30 seconds each.

Printability quantification

When assessing printability, *Pr* is a quantitative parameter used to evaluate the pore geometry of printed scaffolds, based on the perimeter and area of the pore. An ideal *Pr* with high geometric accuracy corresponds to *Pr* = 1 (square shape transversal pore geometry) [2]. A *Pr* value lower than 1 is indicative of poor crosslinking and roundshaped pores, while a *Pr* value higher than 1 indicates irregular-shaped pores. Printability assessment was performed using all IL-dissolved keratin solutions. A CELLINK printer was used (BIOX), equipped with a 25 G needle and a 3mL pneumatic syringe, where the IL solutions were loaded. No additional precursor ink treatment was necessary. 3D models were designed using the printer's software and embedded 3D printing was performed using the previously described support bath and a 25G needle for both solutions. A printing speed of 8 mm×s^{-1} was used throughout and printing pressures were varied from 10 kPa for $[C_2C_1im][C_1CO_2]$ to 35 kPa for $[N_{111(2OH)}][C_1CO_2]$. The scaffolds were maintained in the bath at 37 °C for 48 h, enabling the obtention of a crosslinked network that provided good mechanical resistance to the scaffold. The incubation time was optimized to have fully crosslinked structures with high printing fidelity which did not occur before the 48 hours employed (Figure S8). The scaffolds were then transferred into a petri dish and washed with phosphate-buffered saline (PBS) to remove the excess bath. The collected scaffolds were used for further studies. The printability of diverse structures and geometries with different infill patterns and high structural integrity were evaluated. The filament diameter and printability factor (Equation 1) were calculated to characterise the produced scaffolds. Digital images of printed structures were further processed using ImageJ imaging processing software to measure the circularity of the pores.

$$Printability\ factor = \frac{pore\ perimeter^2}{16 \times pore\ area} \tag{1}$$

Degradation testing

The stability of keratin-based 3D printed scaffolds (of both brown and white feathers) was evaluated by assessing their degradation for 28 days. For this, cylinders of 10 · 10 · 1 mm^3 (4 layers) were printed inside the support bath. After incubation at 37 °C for 48 h, the scaffolds were washed with PBS and transferred to diverse Petri dishes containing PBS to keep the structures completely immersed (~6 mL). The samples were kept at 37 °C throughout the whole assay, and at specific time points (0, 7, 14, 21 and 28), three representative structures of each ink were collected and weighed to determine the remaining mass (wet weight - m_w). Finally, the samples were freeze-dried to obtain the dry weight (m_d) and calculate the remaining mass and water content as represented below:

$$Remaining\ mass\ (\%) = \frac{m_w\ (t_1)}{m_w\ (t_0)} \times 100 \tag{2}$$

$$Water\ content\ (\%) = \frac{m_w\ (t_1) - m_d\ (t_1)}{m_w\ (t_1)} \times 100 \tag{3}$$

Mechanical characterisation

The mechanical properties of the 3D printed scaffolds were assessed using a universal mechanical testing machine (3340 series, INSTRON, USA) equipped with a 50 N load cell in compressive mode. Mechanical testing was performed to assess Young's Modulus (YM), which is related to the capacity of elastic deformation under stress. In this case, cylinders of 10 · 10 · 3 mm^3 (12 layers) in size were 3D printed and retrieved as previously described. Additionally, a bulk (non-porous) form was printed to evaluate the effect of pore voids on the mechanical properties. Compression assays were performed on fresh scaffolds with a diameter of ~8 mm and height of ~2.5 mm, and after 28 day incubation in PBS at 37 °C. Eight samples *per* condition were analysed. The YM was calculated from the stress-strain curve as the maximum slope of the initial linear portion of the curve (5% - 15% of compressive strain), neglecting any toe region due to the initial conditioning of the specimen.

In vitro cytocompatibility studies

Human adipose-derived stem cells (hASCs) were used for *in vitro* cytocompatibility studies. These cells were isolated from human adipose tissue samples obtained from a local hospital under an ethically approved protocol established between the COMPASS research group and Centro Hospitalar do Baixo Vouga. The subjects signed an informed consent and were made fully aware of the right to withdraw consent at any time. The hASCs were cultured in alpha-minimum essential medium (α-MEM, Thermo Fisher), containing 10 % fetal bovine serum (FBS, Thermo Fisher) and 1% antibiotic/antimycotic (Thermo Fisher). The cultures were maintained under a 5% CO_2 atmosphere at 37 °C, with medium replacement every 3 days. Cells between passages 4 and 5 were used for all experiments.

The scaffolds were prepared as previously mentioned and then sterilised with UV light in a flow chamber for 20 min. The structures were transferred to a 48-well plate before being seeded with 10×10^4 cells/well and kept under agitation in a rocking shaker overnight. Cultures were maintained for a total of 7 days, during which specific time points were taken on days 1, 3 and 7. Cells cultured in TCPS were used as controls, and the same number of cells was used for the seeding, in order to have comparable data.

Cellular metabolic activity quantification

AlamarBlue®, a commercially available kit, was used to assess cellular metabolic activity through the quantitative reduction of resazurin. Only viable cells with active metabolism can reduce this compound to resofurin, a pink-soluble compound. This metabolic conversion results in a colour change that can be measured via fluorescence spectroscopy on a microplate reader [3]. The advantage of this assay is that it does not affect the cells, allowing for subsequent assays in the same samples or continued evaluation of the cell culture over time.

On days 1, 3 and 7, the scaffolds (n=4) were incubated with fresh culture medium containing 10 % of AlamarBlue reagent for 4 h at 37 °C. For all conditions, 100 µL of each solution (in triplicate) was used to determine the fluorescence intensity in a microplate reader (Synergy HTX, Biotek, USA) at 540-600 nm. To account for potential background signals, we incubated the scaffolds without cells under the same conditions. The resulting fluorescence values were used as blanks and subtracted from the fluorescence values. Fresh culture media containing 10 % of AlamarBlue reagent without contact with samples was used as a control.

Evaluation of cellular performance

The Live/Dead assay provides a qualitative measurement of cell viability and can be used to complement quantitative assays. Briefly, two independent assays were performed, where the scaffolds (*n* = 4 for each assay) were incubated for 30 min at 37 °C with 300 µL of a staining solution containing Calcein-AM (2 $\mu g \times mL^{-1}$) and propidium iodide (PI) (1 μg×mL^{-1}) in PBS. Following incubation, the scaffolds were washed with PBS and immediately analysed using a fluorescence microscope (Axio Imager 2, Zeiss, Germany). Images of the scaffolds without cells were also acquired and included in the ESI (Fig. S8).

A proliferation assay was performed to determine the distribution of cells by staining cell nuclei with 4′,6-diamidino-2-phenylindole (DAPI) and cell membranes with phalloidin. The constructs were washed three times with PBS and incubated with DAPI (1:1000 v/v) for 20 min. After two washing steps with PBS, the constructs were incubated with phalloidin (1:1000 v/v) for 25 min and washed with PBS. Images were recorded digitally using Confocal Microscopy ZEISS LSM 900 and further processed using Zeiss imaging processing software.

Scanning electron microscopy

Scaffolds used for the asses cellular morphology were analysed by scanning electron microscopy (SEM). First, the samples were dehydrated using an ethanol gradient (50, 70, 80, 90, 95, 97.5, and 100 %, for 20 min in each solution) and dried to the critical point. The samples were then coated with carbon conductive adhesive and analysed in a Hitachi SU-70 (Japan) with an acceleration voltage of 5 kV.

Statistical analysis

Statistical analyses were performed using GraphPad Prism 10 (GraphPad Software, California, USA). Data were expressed as means ± standard deviation of experiments with a minimum of three independent assays. Differences between groups were analysed by two-way analysis of variance (ANOVA). Statistical significance corrections were applied to multiple comparisons. Significance levels between groups were defined as follows: $^{*}p < 0.05$, $^{**}p < 0.01$, $^{***}p < 0.001$, $^{****}p < 0.0001$.

Results and Discussion

Extended Discussion

Keratin and disulfide bonds: A computational simulation performed by Zhang et al.[4] emphasised that acetate-based ILs have a high S-S bond breakage percentage (up to 95 %) [4], resulting in enhanced feather dissolution (as previously demonstrated by our research group [1,5]). According to Kehm et al.[6] proteins are primary targets for oxidation due to their high abundance in cells and extracellular tissues and their rapid reaction rates with oxidants. Keratin is rich in sulphur-containing amino acids such as cysteine and methionine [6,7]. This makes keratin particularly susceptible to oxidative stress, which promotes the formation of disulfide bonds. This bond formation stabilises protein structures through intra- and intermolecular disulfide bridges, being a reversible process [6]. Chen et al. [8] demonstrated the effect of pH on the S-S reforming. At pH 7.4, keratin solutions could not form structures due to insufficient thiol-disulfide exchange, whereas by adjusting the pH to 9.5-10.0, crosslinking occurred. This was attributed to the pKa value of thiol groups in keratin, which is around 8-10, needing an alkaline environment for S-S reformation [8]. Reforming natural S-S is energetically favourable and faster than creating non-natural ones, as previously reported [9].

Support bath elastic recovery rationale: By lowering the strain to 1% in each cycle, it enables the bath to dynamically recover its elastic properties after undergoing significant strains, thereby mimicking the self-healing behaviour of the solution when the printing nozzle is moving inside the bath. If support baths are not able to recover their elasticity immediately, the printing solutions can leak through the open space left by the needle path, leading to printing inaccuracies.

3D printing: The successful printing of the inks was highlighted by the well-preserved details in the 3D models used, including filaments and porosity, demonstrating the robustness of both feathers for 3D printing and reinforcing the simplicity of our approach, eliminating the need of external crosslinking agents in the final ink formulations. Our results underscore the importance of characterising the inks to optimise their properties and adapting the printing process according to the final aims. According to Becker et al.[10] low-viscosity inks are associated with low shape and poor printing fidelity. This leads to significant challenges in achieving complex geometries, resulting in rough surface textures even when granular baths are employed [10]. Thus, the use of an optimised support bath, as herein developed, can lead to better printing results and shape fidelity.

Remaining mass and water content analysis: Regarding quantitative assessment of remaining mass (Fig. 4B), at 28 days, a decrease of 28 – 58 wt% was obtained, varying according to each scaffold. For WF + Ch-IL, most of the mass was lost in the first 7 days (reduction of 30 wt%), without significant loss from day 7 onwards. For BF + Ch-IL, around 12 wt % was lost in the first 7 days, with the most significant reduction at 28 days (35 wt%). Analysing the inks composed of Im-IL, the ink with WF presented the higher loss at 14 days (27 wt%), while the ink with BF resulted in a higher loss in 28 days (60 wt%), corroborating lower crosslinking ability of these inks and the fragile nature of these constructs observed throughout the assays. For the water content analysis (Fig. 4C), minimal differences were obtained. For example, inks from the Ch-IL resulted in (87.77 ± 1.94) wt% (WF) and (90.05 ± 2.06) wt% (BF), while inks from Im-IL resulted in (93.58 ± 1.04) wt% (WF) and (93.48 ± 1.93) wt% (BF), with small fluctuations during the evaluated time. Interestingly, inks containing Im-IL exhibit higher water content, which can be attributed to less effective crosslinking compared to those formed with Ch-IL (as mentioned before). In summary, IL-dissolved keratin inks can be readily tailored for different applications, including tissue engineering implants, since they can maintain stability over time. Nevertheless, excessive water content can result in impaired mechanical properties [11].

Effect of melanin on cellular behavior: Melanin is a ubiquitous material found in mammals, birds, and insects. In humans, melanin is synthesised by melanocytes and acts like a UV-protective agent for keratinocytes at the epidermis layer of the skin, while keratin is the protein that comprises most of this skin layer [12]. This can explain the initial difficulty in cell adherence on BF scaffolds, since there is a lower keratin concentration on these formulations. When melanin is present, cell-cell interactions are preferable over cell-material interactions, at least during the first days of culture. Therefore, melanin in BF could have a potential role in modulating cell adhesion, metabolic activity and migration, besides its natural pigmentation role, which could be tailored for every skin colour.

Metabolic activity of keratin-based materials and commercially available (bio)inks: Bedir et al.[13] investigated the metabolic activity of GelMA-KerMA hydrogels across 1, 3, and 7 days of incubation, confirming a progressive increase in cell viability overtime [13]. Similarly, Yu et al.[14] evaluated the metabolic activity in KEMA:GCMA hydrogels over 1, 3, and 5 days, also revealing a notable increase in cell proliferation and widespread distribution as the culture period extended. Furthermore, their evaluation of varying keratin concentrations demonstrated that hydrogels with higher keratin content exhibited increased cell migration and proliferation, underscoring the potential of keratin in promoting hASC adhesion, proliferation and differentiation [14]. In comparison to commercially available (bio)inks, such as CELLINK® GelMA A, CELLINK® GelXA FIBRIN and CELLINK® FIBRIN, our construct demonstrated similar or superior cytocompatibility. For instance, Ronzoni et al.[15] reported cell viability of 94% for these inks over 14 days in culture. Similarly, Loi et al.[16] used fibrinogen-based hydrogel (CELLINK®) and reported cell viabilities >94%. Stocco et al.[17] evaluated a type I collagen bioink (Lifeink® 200, Advanced BioMatrix) and reported cell viability >80% after 1 and 7 days. Taken together, these comparisons highlight the excellent performance of our material in supporting cell viability and metabolic function.

Clinical feasibility and scalability of the developed solutions: Herein, a direct and innovative method for producing IL-based personalised scaffolds was described, taking advantage of chicken feather waste valorisation. Considering the large amount of feather waste generated annually worldwide, this strategy offers a sustainable solution for the valorisation of an abundant, low-cost and underutilised biomass. Although this study demonstrates a sustainable and effective strategy for keratin-based scaffold processing, further investigations are needed to ensure clinical feasibility. The scaffolds were sterilized by ultraviolet (UV) light exposure for 20 min prior to biological testing, with no adverse effects observed in cell viability or morphology. This sterilization method has also been successfully applied to keratin-based films developed by our group for wound healing applications [1]. The raw material (chicken feathers) was subjected to an initial cleaning process, including immersion in ethanol for 24 h, followed by dissolution in ILs at 100 °C for 4 hours - a condition that contributes to the inactivation of surface pathogens and potential antigens. These combined steps help ensure the biocompatibility and safety of the resulting material. The most promising solvent in this study ($[N_{111(2OH)}][C_1CO_2]$) is based on a cholinium cation that can be derived from natural sources, offering the possibility of employing a bio-based and biocompatible IL. Nevertheless, *in vivo* safety assessments will be required to meet regulatory certifications for biomedical applications. Furthermore, biomass variability can affect keratin yield and properties, which are highly relevant when considering large-scale production. Future scale-up efforts should include standardization protocols, quality control measures and batch blending when necessary.

Supplementary Figures

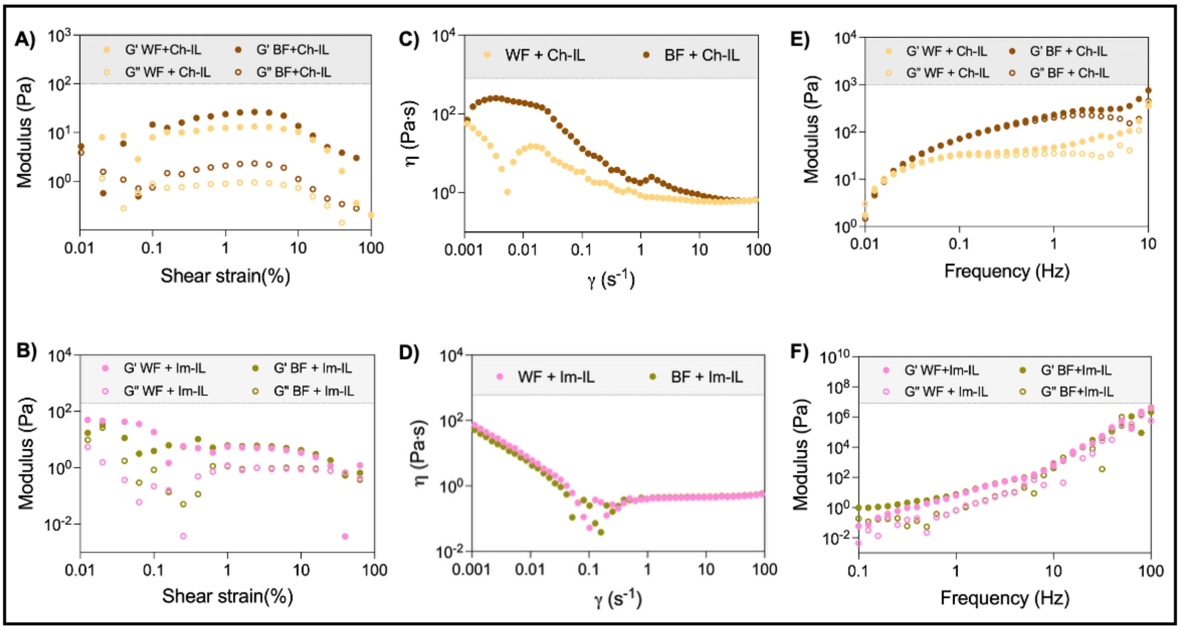

Fig. S1 Rheological analysis of IL-based inks. (A) shear rate sweep of WF + Ch-IL and BF + Ch-IL (B) and of WF + Im-IL and BF + Im-IL, (C) strain sweep of WF + Ch-IL and BF + Ch-IL, (D) and of WF + Im-IL and BF + Im-IL, (E) frequency sweep of WF + Ch-IL and BF + Ch-IL and (F) and of WF + Im-IL and BF + Im-IL.

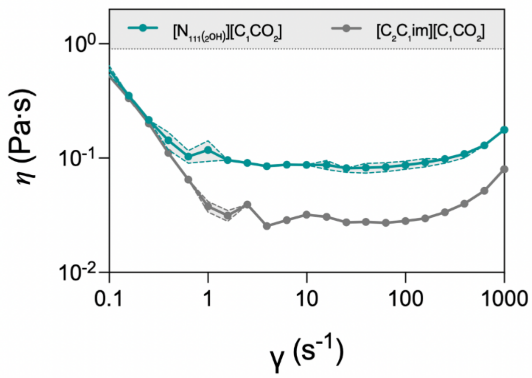

Fig. S2 Shear-thinning behaviour of aqueous solutions of $[N_{111(2OH)}][C_1CO_2]$ (Ch-IL) and $[C_2C_1im][C_1CO_2]$ (Im-IL) (80 wt% ionic liquid in water).

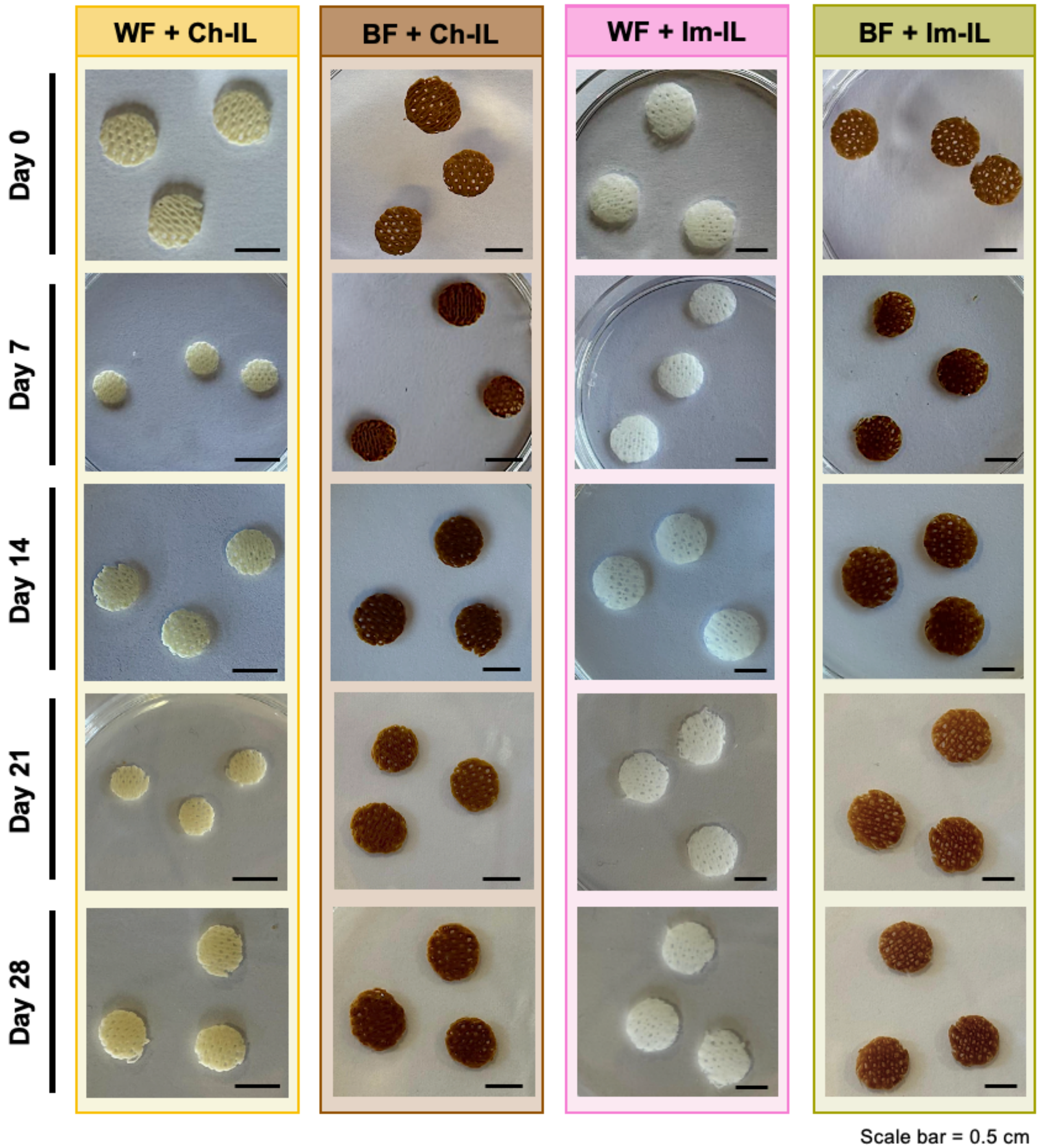

Fig. S3 Printability evaluation using different geometries and their integrity evaluation after removal from the support bath using cylinder geometries with 4 layers.

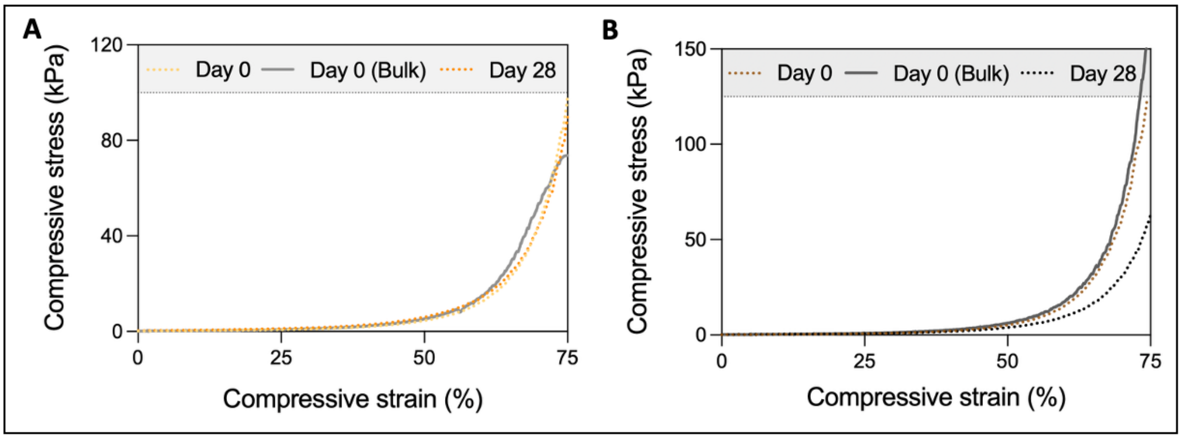

Fig. S4 Compressive modulus of the scaffolds produced from white and brown feathers dissolved in $[N_{111(2OH)}][C_1CO_2]$ (n = 5).

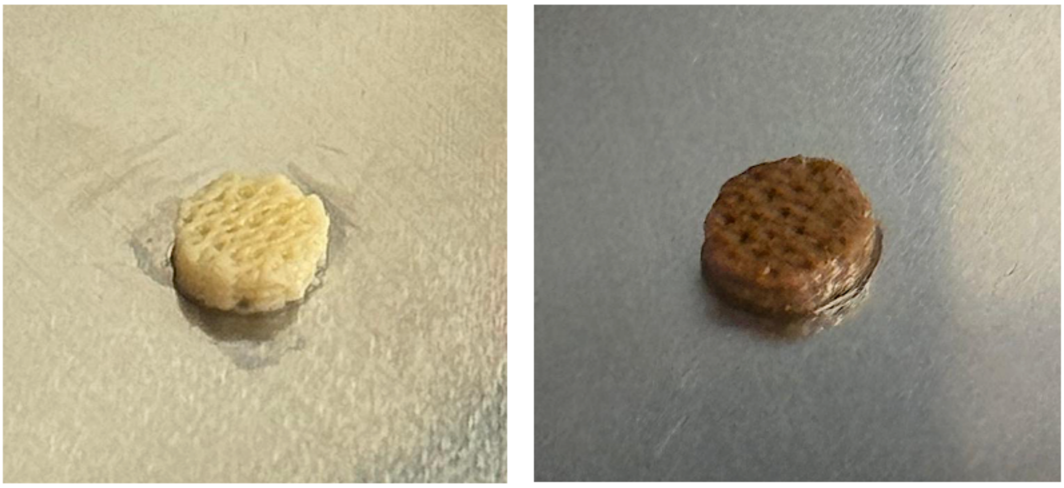

Fig. S5 Macroscopic appearance of scaffolds incubated in PBS at 37 °C for 28 days (no cell contact).

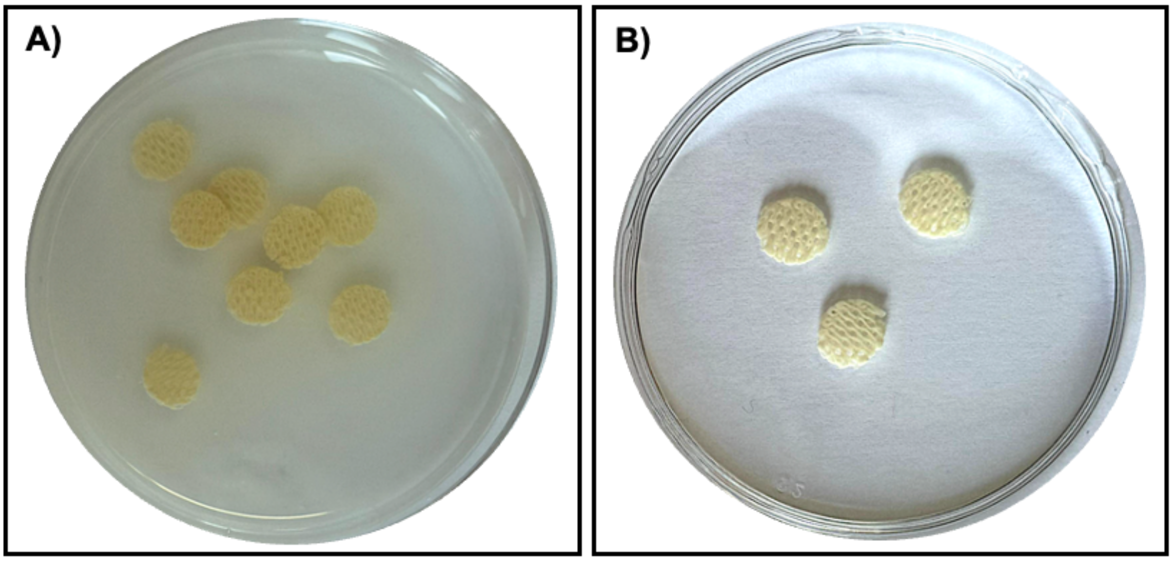

Fig. S6 Printed scaffolds within the support bath and (B) scaffolds after the removal from the support bath and within PBS.

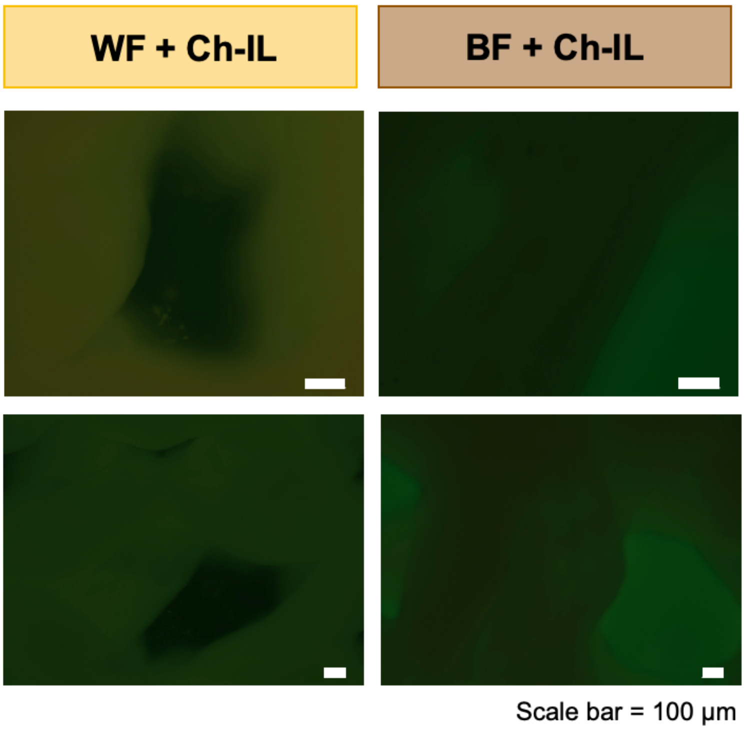

Fig. S7 LIVE/DEAD staining of scaffolds cultured without cells.

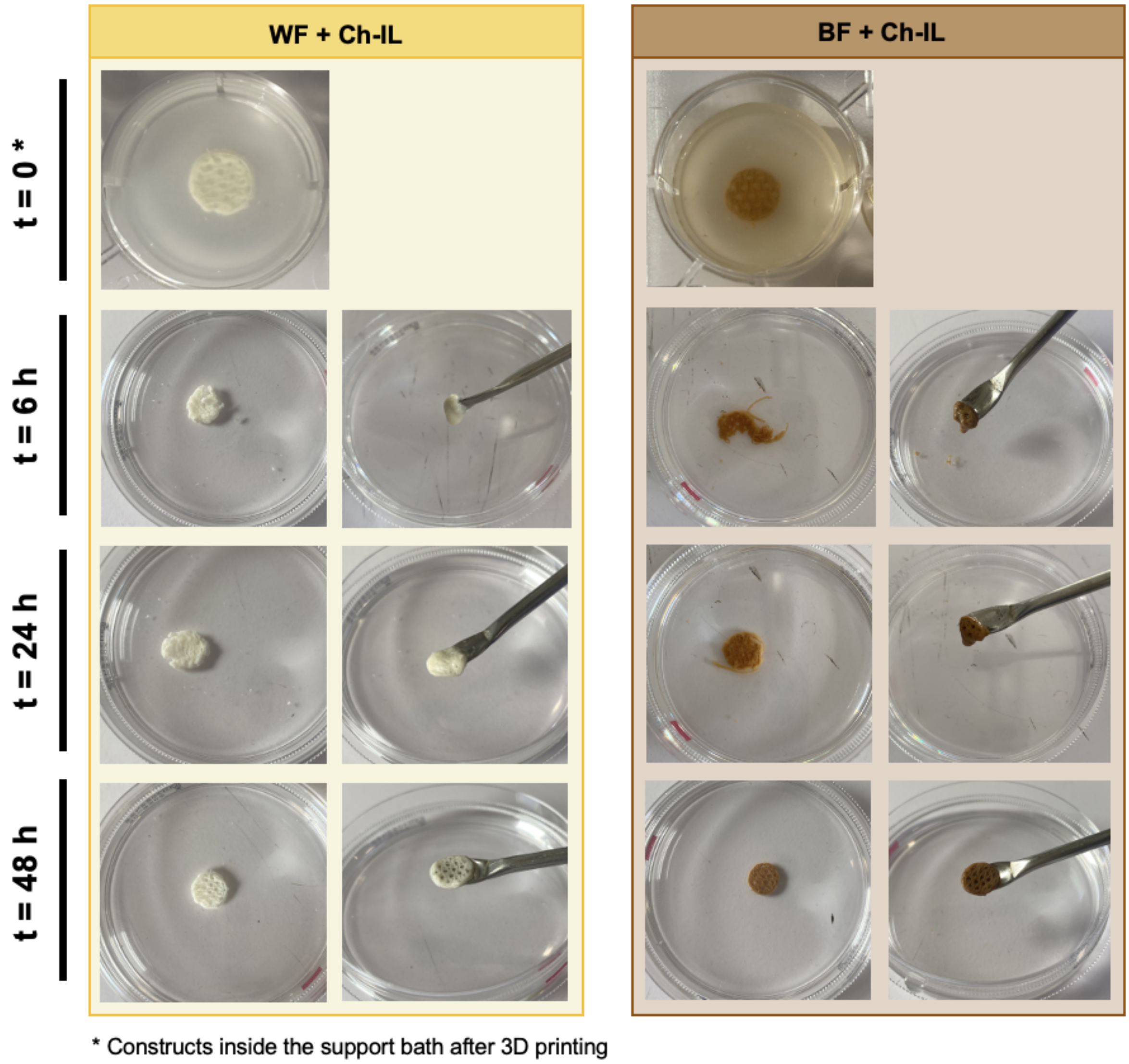

Fig. S8 Time-dependent evolution of scaffolds crosslinking, with complete crosslinking observed at 48 h.

[Click here to visualize Video S1]

Video S1 3D printing of a chicken feather model.

[Click here to visualize Video S2]()

Video S2 3D printing procedure in a well plate for biological assays.

References

(1) Polesca, C.; Passos, H.; Neves, B. M.; Coutinho, J. A. P.; Freire, M. G. Valorization of Chicken Feathers Using Aqueous Solutions of Ionic Liquids. *Green Chemistry* **2023**, *25*, 1424–1434. https://doi.org/10.1039/D2GC04477C.

(2) Schwab, A.; Levato, R.; D'Este, M.; Piluso, S.; Eglin, D.; Malda, J. Printability and Shape Fidelity of Bioinks in 3D Bioprinting. *Chemical Reviews*. American Chemical Society October 14, 2020, pp 11028–11055. https://doi.org/10.1021/acs.chemrev.0c00084.

(3) Maia, J. R.; Castanheira, E.; Rodrigues, J. M. M.; Sobreiro-Almeida, R.; Mano, J. F. Engineering Natural Based Nanocomposite Inks via Interface Interaction for Extrusion 3D Printing. *Methods* **2023**, *212*, 39–57. https://doi.org/10.1016/j.ymeth.2023.03.001.

(4) Zhang, Z.; Nie, Y.; Zhang, Q.; Liu, X.; Tu, W.; Zhang, X.; Zhang, S. Quantitative Change in Disulfide Bonds and Microstructure Variation of Regenerated Wool Keratin from Various Ionic Liquids. *ACS Sustain Chem Eng* **2017**, *5* (3), 2614–2622. https://doi.org/10.1021/acssuschemeng.6b02963.

(5) Polesca, C.; Al Ghatta, A.; Passos, H.; Coutinho, J. A. P.; Hallett, J. P.; Freire, M. G. Sustainable Keratin Recovery Process Using a Bio-Based Ionic Liquid Aqueous Solution and Its Techno-Economic Assessment. *Green Chemistry* **2023**. https://doi.org/10.1039/D3GC00850A.

(6) Kehm, R.; Baldensperger, T.; Raupbach, J.; Höhn, A. Protein Oxidation - Formation Mechanisms, Detection and Relevance as Biomarkers in Human Diseases. *Redox Biology*. Elsevier B.V. June 1, 2021. https://doi.org/10.1016/j.redox.2021.101901.

(7) Resetco, C.; Hendriks, B.; Badi, N.; Du Prez, F. Thiol-Ene Chemistry for Polymer Coatings and Surface Modification-Building in Sustainability and Performance. *Materials Horizons*. Royal Society of Chemistry November 1, 2017, pp 1041–1053. https://doi.org/10.1039/c7mh00488e.

(8) Chen, M.; Ren, X.; Dong, L.; Li, X.; Cheng, H. Preparation of Dynamic Covalently Crosslinking Keratin Hydrogels Based on Thiol/Disulfide Bonds Exchange Strategy. *Int J Biol Macromol* **2021**, *182*, 1259–1267. https://doi.org/10.1016/j.ijbiomac.2021.05.057.

(9) Gomes, M. C.; Pinho, A. R.; Custódio, C.; Mano, J. F. Self-Assembly of Platelet Lysates Proteins into Microparticles by Unnatural Disulfide Bonds for Bottom-Up Tissue Engineering. *Advanced Materials* **2023**, *35* (41). https://doi.org/10.1002/adma.202304659.

(10) Becker, M.; Gurian, M.; Schot, M.; Leijten, J. Aqueous Two-Phase Enabled Low Viscosity 3D (LoV3D) Bioprinting of Living Matter. *Advanced Science* **2023**, *10* (8). https://doi.org/10.1002/advs.202204609.

(11) Noshadi, I.; Walker, B. W.; Portillo-Lara, R.; Sani, E. S.; Gomes, N.; Aziziyan, M. R.; Annabi, N. Engineering Biodegradable and Biocompatible Bio-Ionic Liquid Conjugated Hydrogels with Tunable Conductivity and Mechanical Properties. *Sci Rep* **2017**, *7* (1). https://doi.org/10.1038/s41598-017-04280-w.

(12) Nowogrodski, C.; Damatov, Y.; Sapru, S.; Shoseyov, O. In Situ Synthesis of Keratin and Melanin Chromophoric Submicron Particles. *ACS Omega* **2023**, *8* (30), 26762–26774. https://doi.org/10.1021/acsomega.3c00189.
(13) Bedir, T.; Baykara, D.; Yildirim, R.; Calikoglu Koyuncu, A. C.; Sahin, A.; Kaya, E.; Tinaz, G. B.; Insel, M. A.; Topuzogulları, M.; Gunduz, O.; Ustundag, C. B.; Narayan, R. Three-Dimensional-Printed GelMA-KerMA Composite Patches as an Innovative Platform for Potential Tissue Engineering of Tympanic Membrane Perforations. *Nanomaterials* **2024**, *14* (7). https://doi.org/10.3390/nano14070563.
(14) Yu, K. F.; Lu, T. Y.; Li, Y. C. E.; Teng, K. C.; Chen, Y. C.; Wei, Y.; Lin, T. E.; Cheng, N. C.; Yu, J. Design and Synthesis of Stem Cell-Laden Keratin/Glycol Chitosan Methacrylate Bioinks for 3D Bioprinting. *Biomacromolecules* **2022**, *23* (7), 2814–2826. https://doi.org/10.1021/acs.biomac.2c00191.
(15) Ronzoni, F. L.; Aliberti, F.; Scocozza, F.; Benedetti, L.; Auricchio, F.; Sampaolesi, M.; Cusella, G.; Redwan, I. N.; Ceccarelli, G.; Conti, M. Myoblast 3D Bioprinting to Burst in Vitro Skeletal Muscle Differentiation. *J Tissue Eng Regen Med* **2022**, *16* (5), 484–495. https://doi.org/10.1002/term.3293.
(16) Loi, G.; Scocozza, F.; Aliberti, F.; Rinvenuto, L.; Cidonio, G.; Marchesi, N.; Benedetti, L.; Ceccarelli, G.; Conti, M. 3D Co-Printing and Substrate Geometry Influence the Differentiation of C2C12 Skeletal Myoblasts. *Gels* **2023**, *9* (7). https://doi.org/10.3390/gels9070595.
(17) Stocco, T. D.; Silva, M. C. M.; Corat, M. A. F.; Lima, G. G.; Lobo, A. O. Towards Bioinspired Meniscus-Regenerative Scaffolds: Engineering a Novel 3D Bioprinted Patient-Specific Construct Reinforced by Biomimetically Aligned Nanofibers. *Int J Nanomedicine* **2022**, *17*, 1111–1124. https://doi.org/10.2147/IJN.S353937.